Feasibility-driven Design of Reflectarrays through Non-Radiating Currents

M. Salucci, G. Oliveri, and A. Massa

Contents

Part I

Numerical Analysis

1 Phase Range [-135:135] - Test Case 1 - 55x55 - Linear Polarization

1.1 K=2000, P=250, I=100000

In the Fig. 1 is depicted the behaviour of the Cost Function varying the random seed. The best value of cost function is achieved by Seed=2 and is $\Phi = 5.414 \times 10^{-2}$.

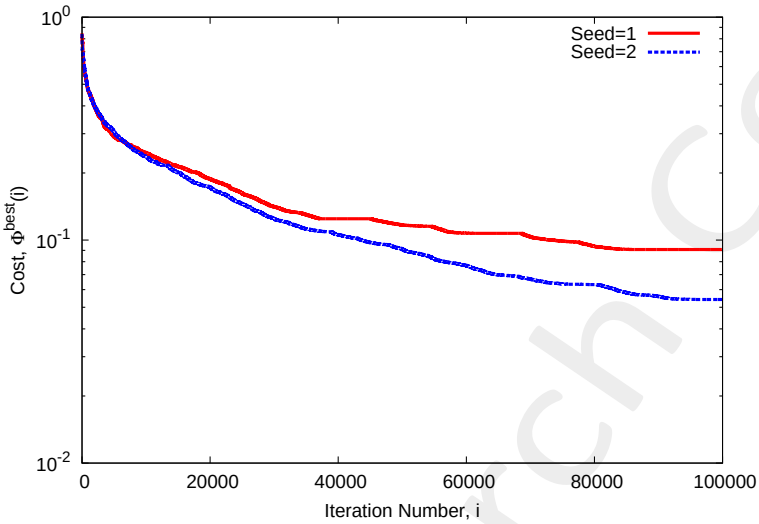

Figure 1: Cost Function behaviour at different random seed.

At this value of cost function the achieved performance on the Phase are showed in Fig. 2 and are numerically showed in table I.

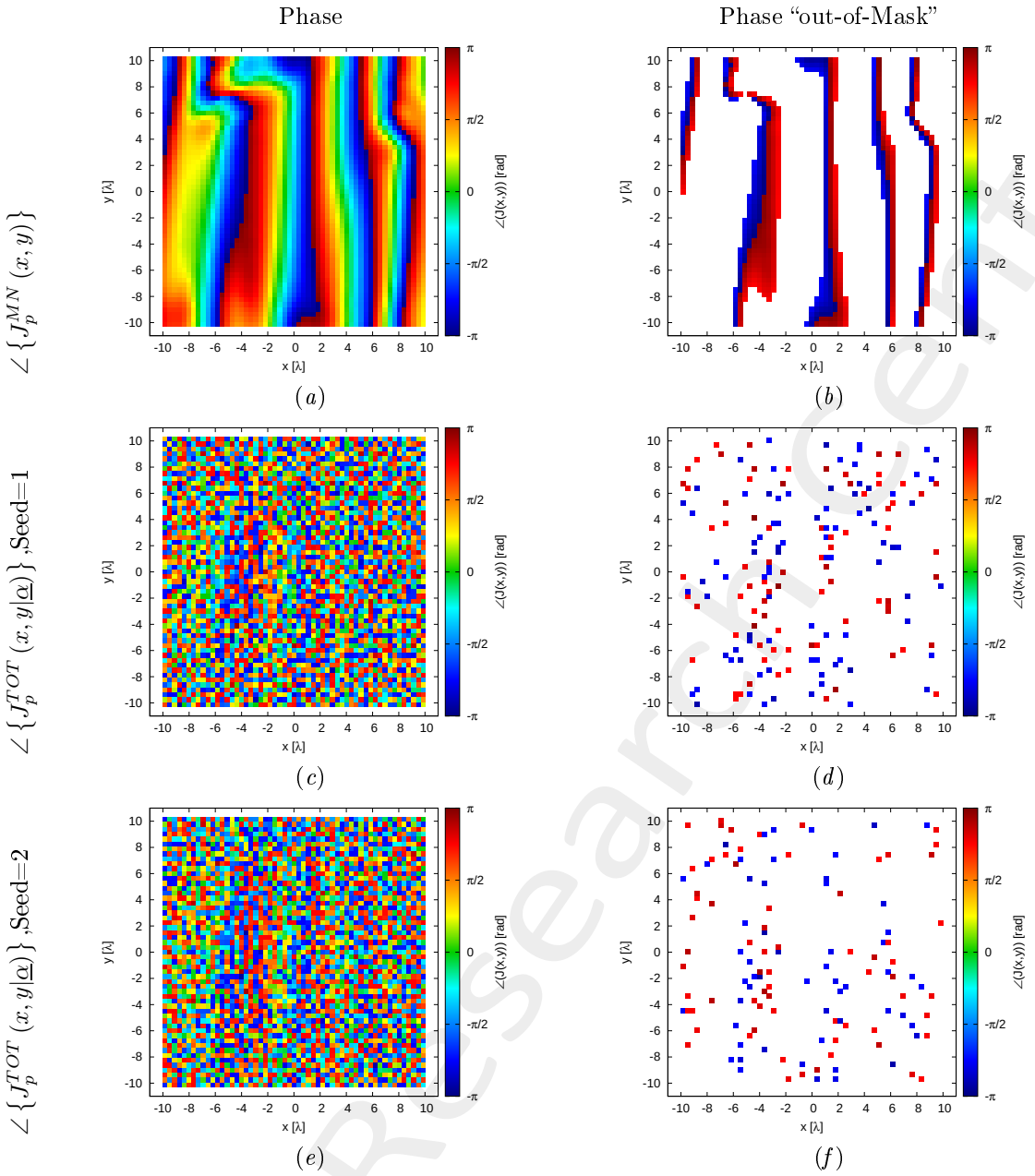

Figure 2: Phase $(a)(c)(e)$ and value of the phase out of the minimization range $(b)(d)(f)$ of the Minimum-Norm current $(\angle\{J_p^{MN}(x,y)\})(a)(b)$, of the total current for the random seed $= 1(c)(d)$ and for the random seed $= 2(e)(f)$.

Case	Φ	Number of value $> \phi_p^{MAX}(x,y)$	Number of value$< \phi_p^{MIN}(x,y)$	Phase Range		Time $[s]$	
				Min $[deg]$	Max $[deg]$	parallel	no-parallel
MN	1.0	451	358	-179.87	179.63		
Seed=1	9.071×10^{-2}	81	88	-169.61	175.37	2.53×10^5	1.42×10^6
Seed=2	5.414×10^{-2}	68	56	-167.54	165.30	2.40×10^5	1.42×10^6

Table I: Cost Function value and statistics about the result.

The verification of the radiated field is showed in Fig. 3 and numerically in table II.

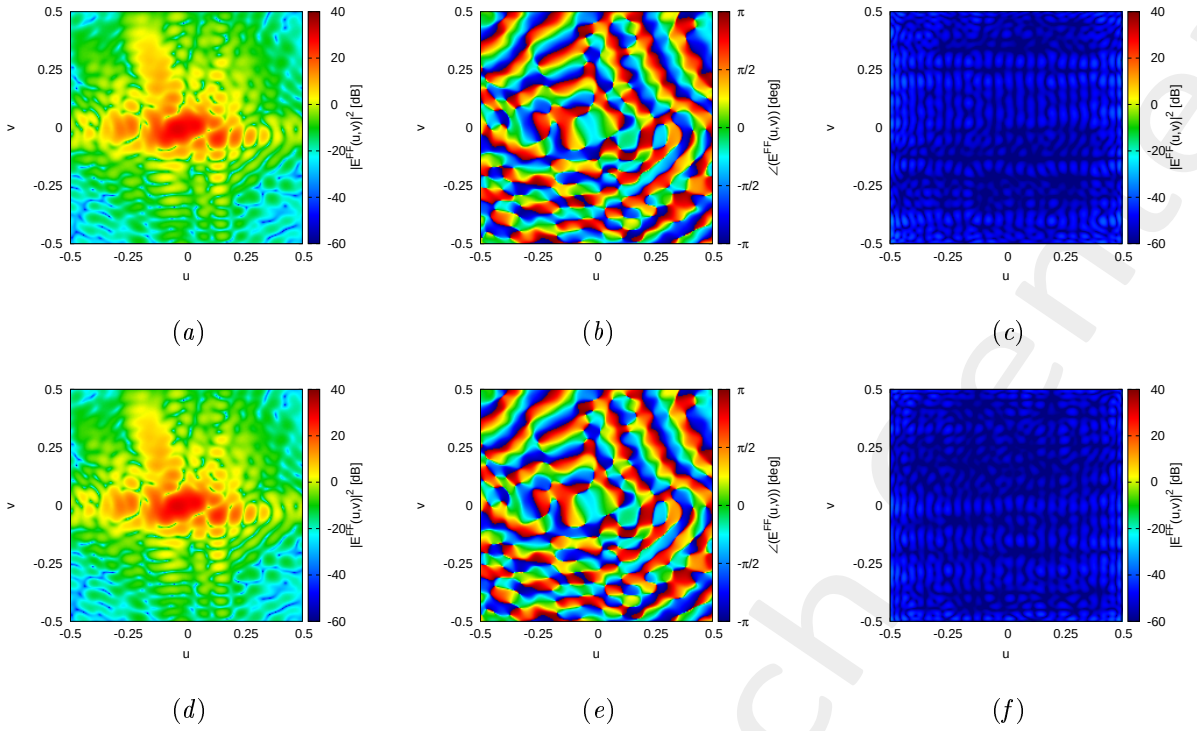

Figure 3: Magnitude $(a)(d)$, Phase $(b)(e)$ and Magnitude of the difference with respect to the original field $(c)(f)$ of the seed=1 $(a)(b)(c)$ and seed=2 $(d)(e)(f)$.

Seed	ξ
1	2.14×10^{-3}
2	1.82×10^{-3}

Table II: Integral error of the difference between the original field and the one radiated by the total current.

1.2 K=2000, P=500, I=100000

In the Fig. 7 is depicted the behaviour of the Cost Function varying the random seed. The best value of cost function is achieved by Seed=2 and is $\Phi = 2.216 \times 10^{-2}$.

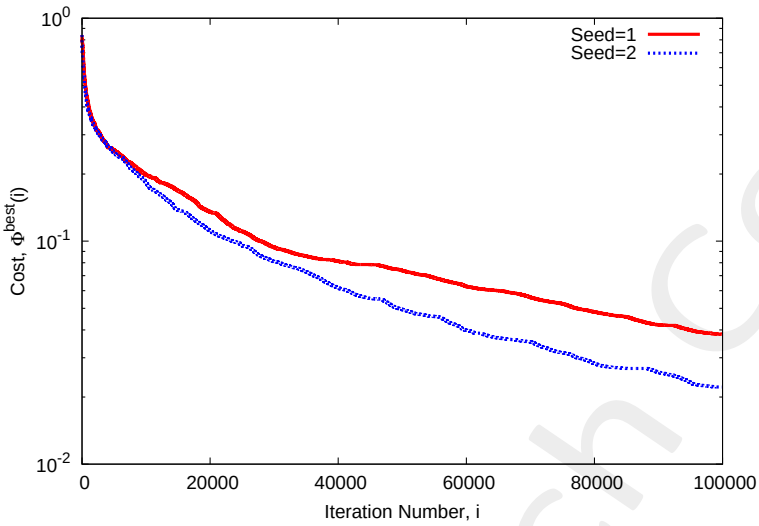

Figure 4: Cost Function behaviour at different random seed.

At this value of cost function the achieved performance on the Phase are showed in Fig. 5 and are numerically showed in table III.

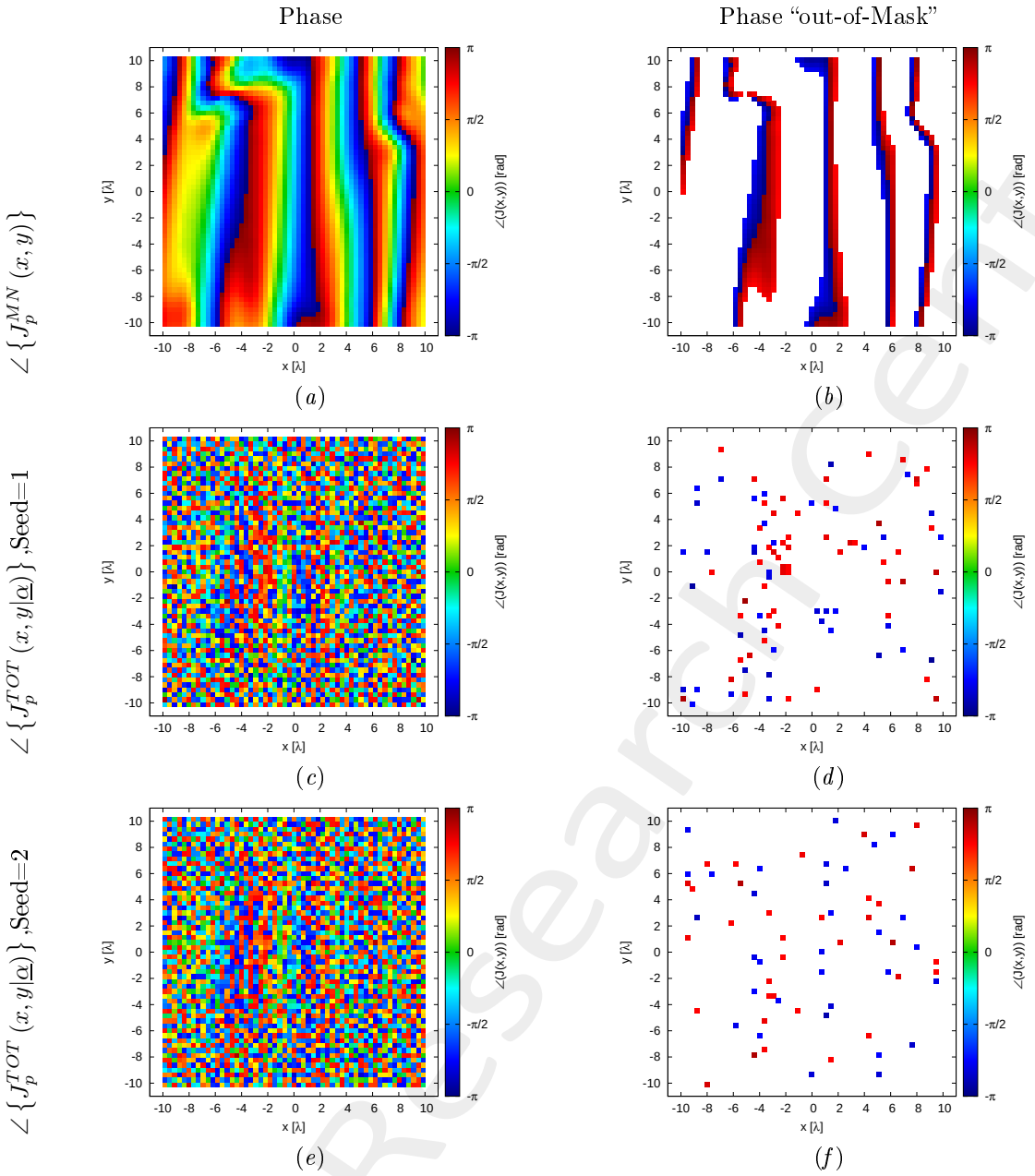

Figure 5: Phase $(a)(c)(e)$ and value of the phase out of the minimization range $(b)(d)(f)$ of the Minimum-Norm current ($\angle\{J_p^{MN}(x,y)\}$)$(a)(b)$, of the total current for the random seed $= 1(c)(d)$ and for the random seed $= 2(e)(f)$.

Case	Φ	Number of value $> \phi_p^{MAX}(x,y)$	Number of value$< \phi_p^{MIN}(x,y)$	Phase Range		Time $[s]$	
				Min $[deg]$	Max $[deg]$	parallel	no-parallel
MN	1.0	451	358	-179.87	179.63		
Seed=1	3.823×10^{-2}	54	43	-171.58	167.27	3.62×10^5	2.83×10^6
Seed=2	2.216×10^{-2}	34	32	-163.47	163.72	3.72×10^5	2.85×10^6

Table III: Cost Function value and statistics about the result.

The verification of the radiated field is showed in Fig. 6 and numerically in table IV.

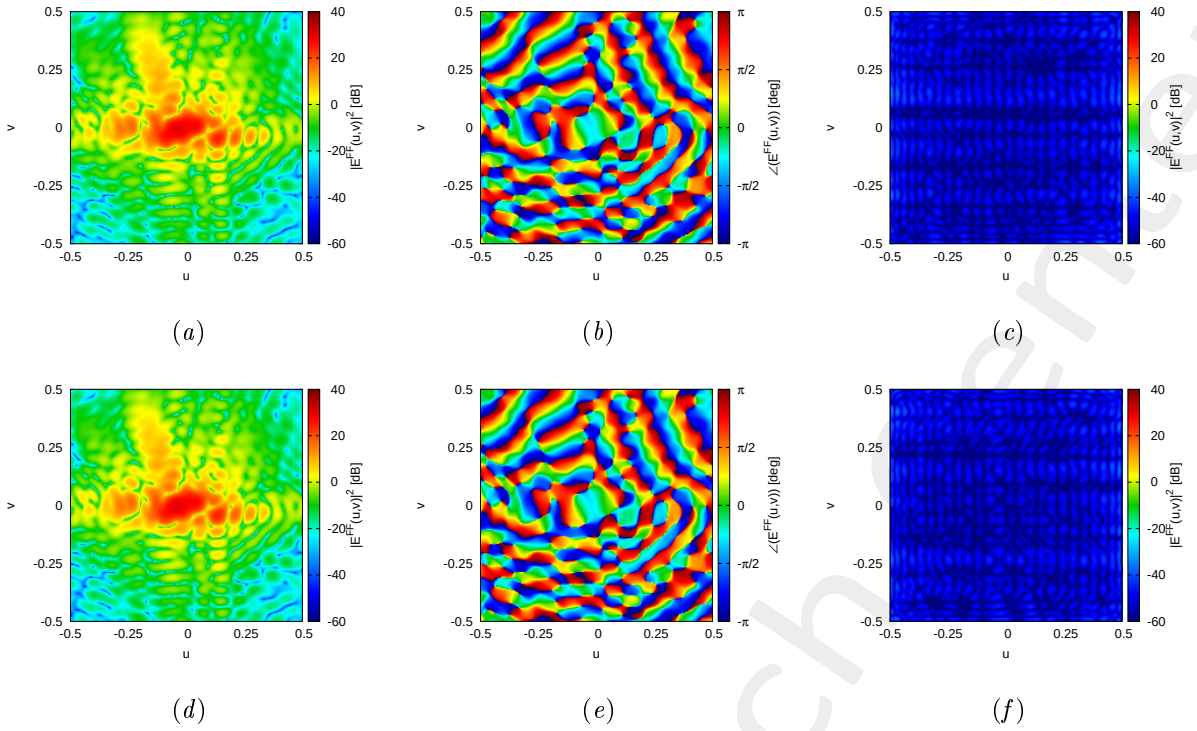

Figure 6: Magnitude $(a)(d)$, Phase $(b)(e)$ and Magnitude of the difference with respect to the original field $(c)(f)$ of the seed=1 $(a)(b)(c)$ and seed=2 $(d)(e)(f)$.

Seed	ξ
1	2.05×10^{-3}
2	2.05×10^{-3}

Table IV: Integral error of the difference between the original field and the one radiated by the total current.

1.3 K=2000, P=1000, I=100000

In the Fig. 7 is depicted the behaviour of the Cost Function varying the random seed. The best value of cost function is achieved by Seed=2 and is $\Phi = 1.325 \times 10^{-2}$.

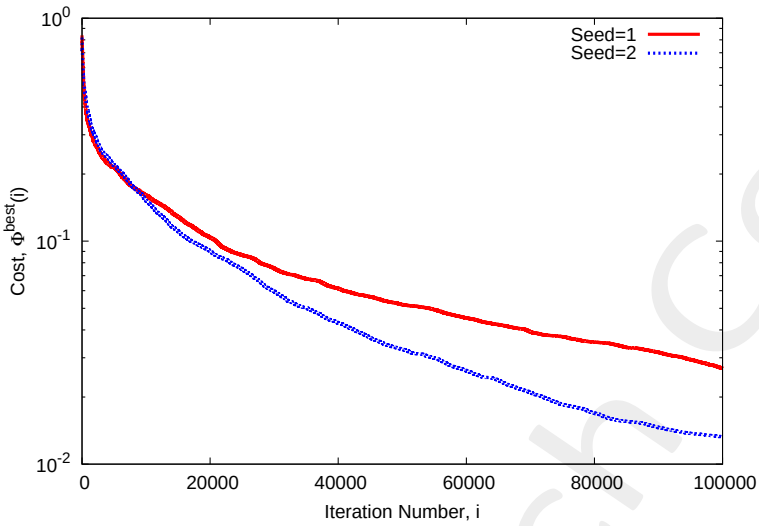

Figure 7: Cost Function behaviour at different random seed.

At this value of cost function the achieved performance on the Phase are showed in Fig. 8 and are numerically showed in table V.

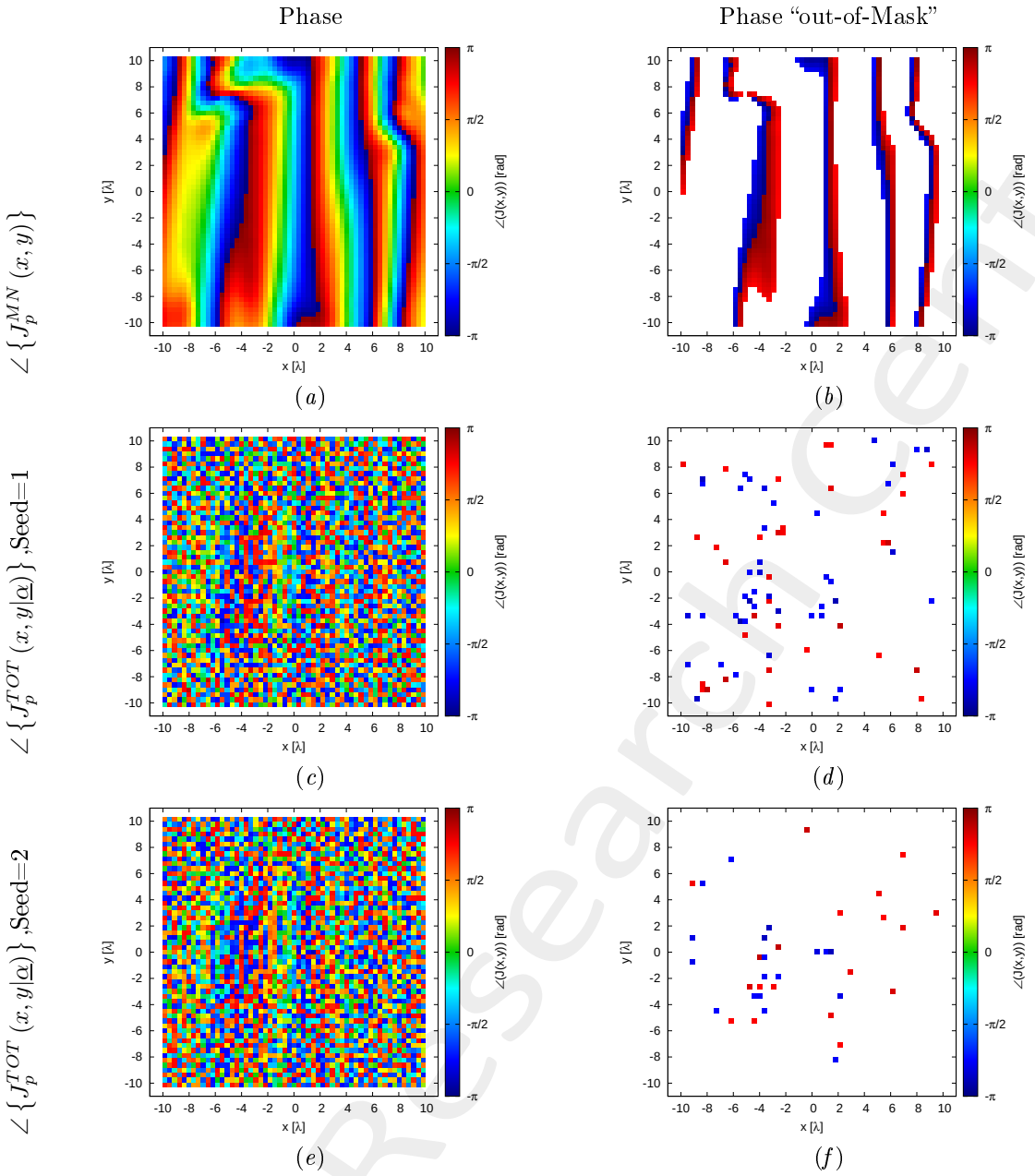

Figure 8: Phase $(a)(c)(e)$ and value of the phase out of the minimization range $(b)(d)(f)$ of the Minimum-Norm current $(\angle\{J_p^{MN}(x,y)\})(a)(b)$, of the total current for the random seed $= 1(c)(d)$ and for the random seed $= 2(e)(f)$.

Case	Φ	Number of value $> \phi_p^{MAX}(x,y)$	Number of value$< \phi_p^{MIN}(x,y)$	Phase Range		Time $[s]$	
				Min $[deg]$	Max $[deg]$	parallel	no-parallel
MN	1.0	451	358	-179.87	179.63		
Seed=1	2.691×10^{-2}	35	44	-162.39	157.60	7.37×10^5	5.65×10^6
Seed=2	1.325×10^{-2}	19	18	-158.25	156.92	8.11×10^5	5.67×10^6

Table V: Cost Function value and statistics about the result.

The verification of the radiated field is showed in Fig. 9 and numerically in table VI.

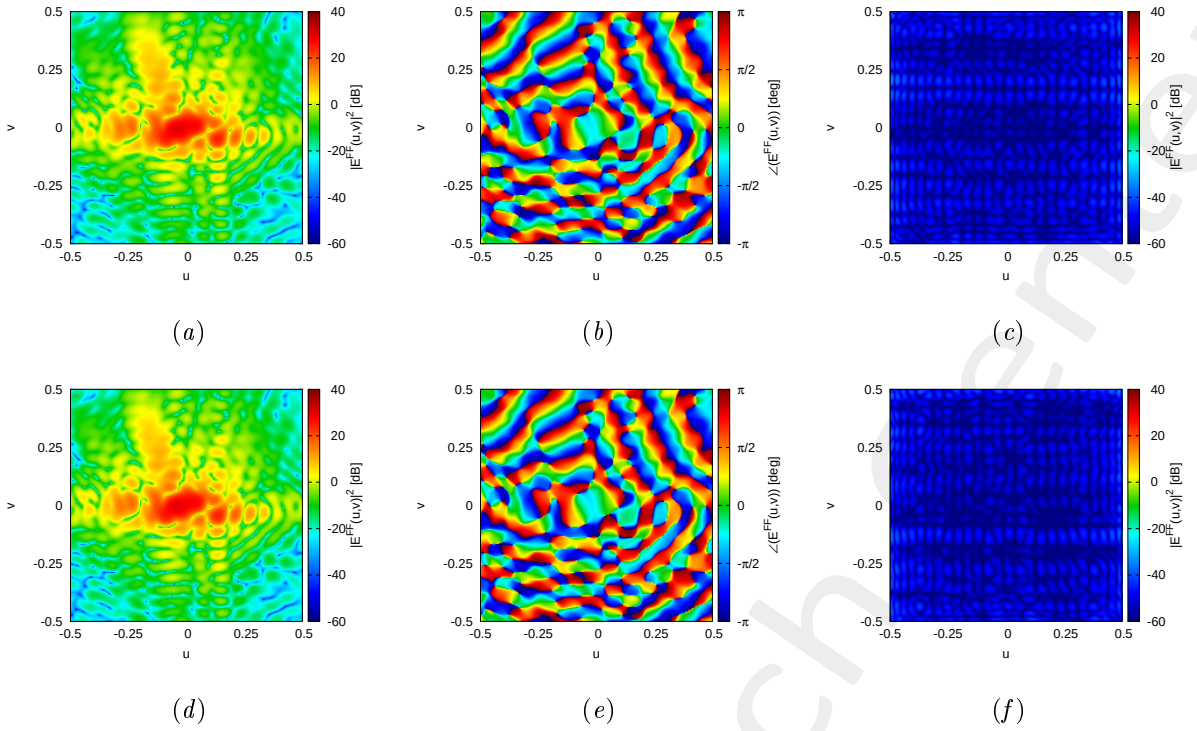

Figure 9: Magnitude $(a)(d)$, Phase $(b)(e)$ and Magnitude of the difference with respect to the original field $(c)(f)$ of the seed=1 $(a)(b)(c)$ and seed=2 $(d)(e)(f)$.

Seed	ξ
1	1.98×10^{-3}
2	1.84×10^{-3}

Table VI: Integral error of the difference between the original field and the one radiated by the total current.

1.4 K=2337, P=467, I=300000

In the Fig. 10 is depicted the behaviour of the Cost Function varying the random seed. The best value of cost function is achieved by Seed=2 and is $\Phi = 6.266 \times 10^{-3}$.

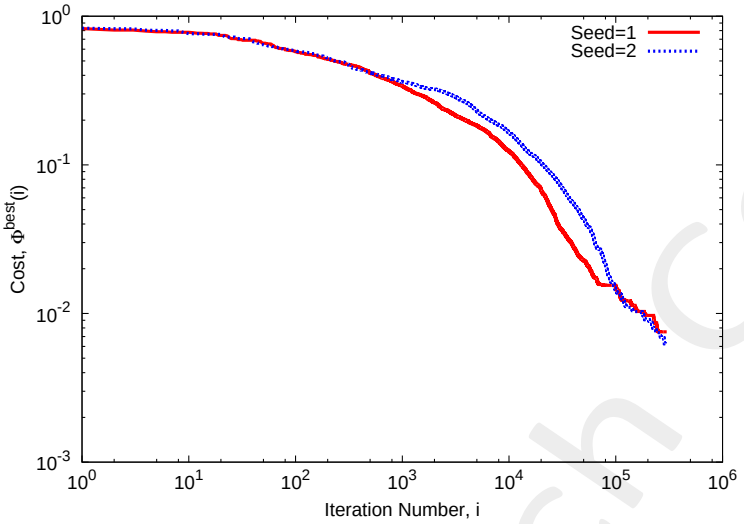

Figure 10: Cost Function behaviour at different random seed.

At this value of cost function the achieved performance on the Phase are showed in Fig. 11 and are numerically showed in table VII.

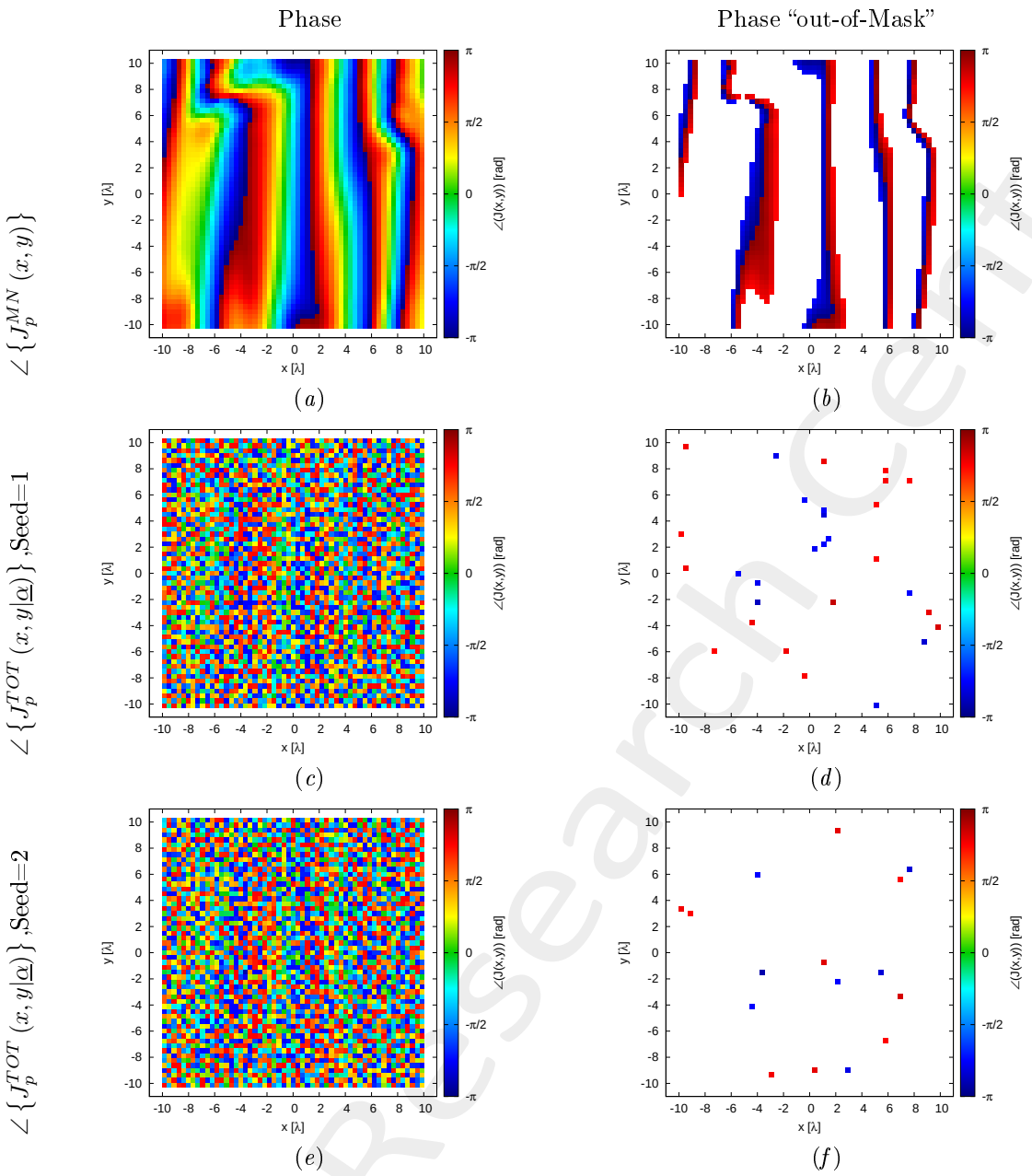

Figure 11: Phase $(a)(c)(e)$ and value of the phase out of the minimization range $(b)(d)(f)$ of the Minimum-Norm current ($\angle\{J_p^{MN}(x,y)\}$)$(a)(b)$, of the total current for the random seed $= 1(c)(d)$ and for the random seed $= 2(e)(f)$.

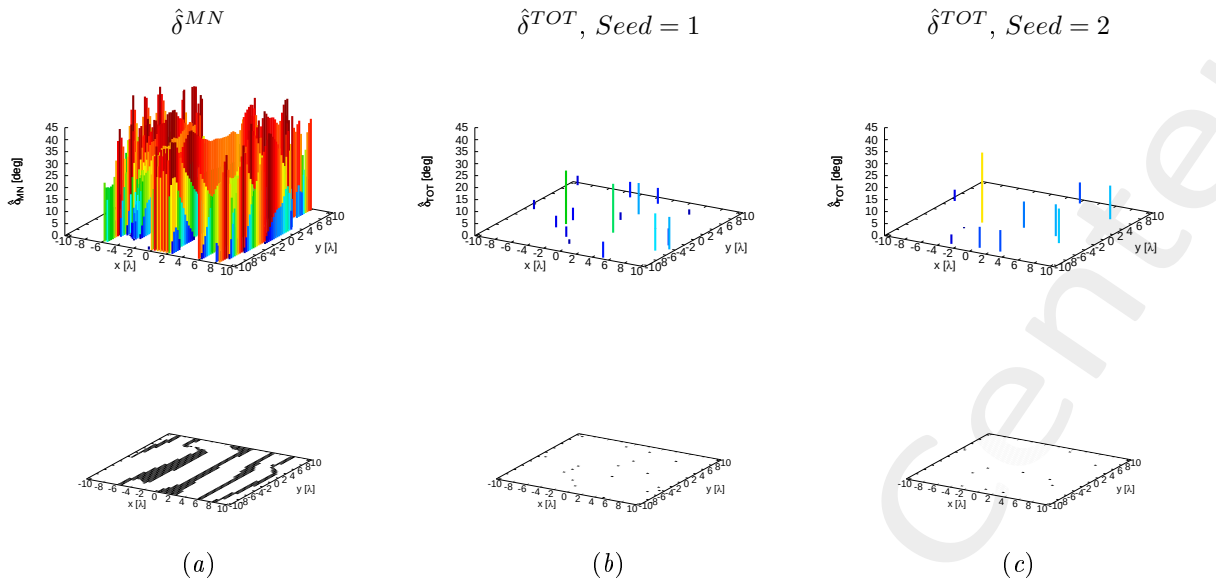

(a) (b) (c)

Figure 12: Phase Mask mismatch for the Minimum-Norm current (a), the total current for the random seed $= 1(b)$, and for the random seed $= 2(c)$.

Case	Φ	Number of value $> \phi_p^{MAX}(x,y)$	Number of value $< \phi_p^{MIN}(x,y)$	Phase Range		Time $[s]$
				Min $[deg]$	Max $[deg]$	
MN	1.0	451	358	-179.87	179.63	
Seed=1	7.531×10^{-3}	16	13	-157.26	155.35	1.18×10^6
Seed=2	6.266×10^{-3}	9	7	-164.20	149.41	1.18×10^6

Table VII: Cost Function value and statistics about the result.

The verification of the radiated field is showed in Fig. 13 and numerically in table VIII.

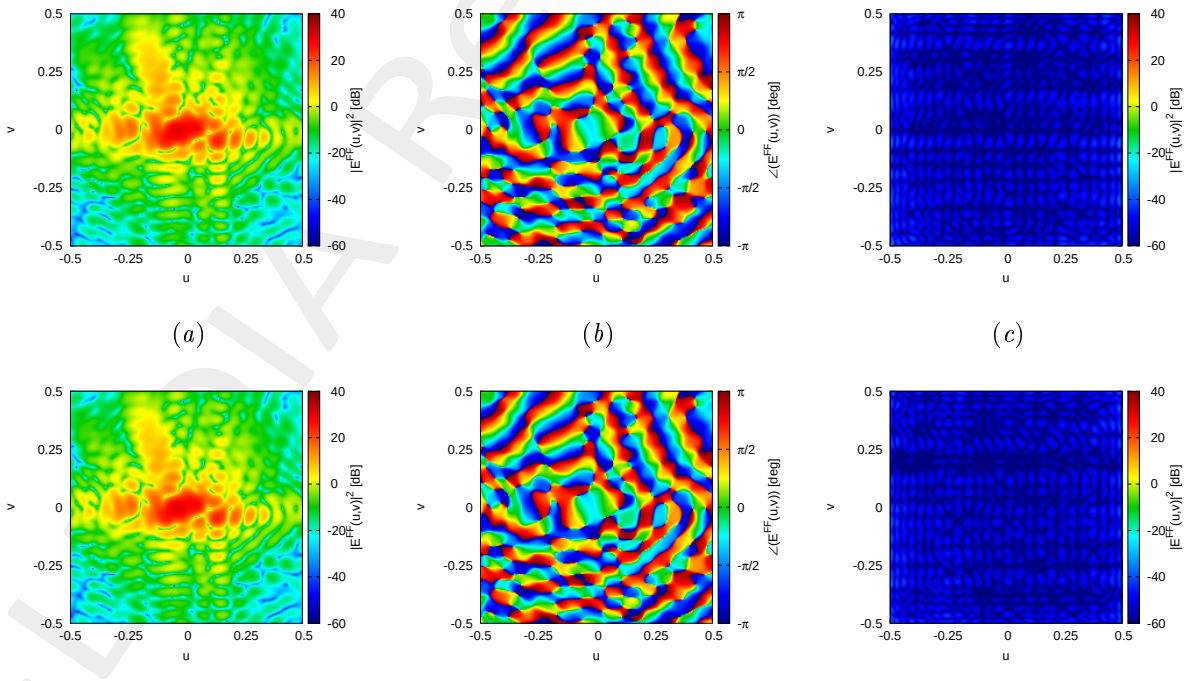

(a) (b) (c)

(d) (e) (f)

Figure 13: Magnitude $(a)(d)$, Phase $(b)(e)$ and Magnitude of the difference with respect to the original field $(c)(f)$ of the seed=1 $(a)(b)(c)$ and seed=2 $(d)(e)(f)$.

Seed	ξ
1	1.83×10^{-3}
2	1.75×10^{-3}

Table VIII: Integral error of the difference between the original field and the one radiated by the total current.

1.5 Comparison

In the Fig. 14 is depicted a summary of the behaviour of the cost function at diffenent population and number of coefficient and seed.

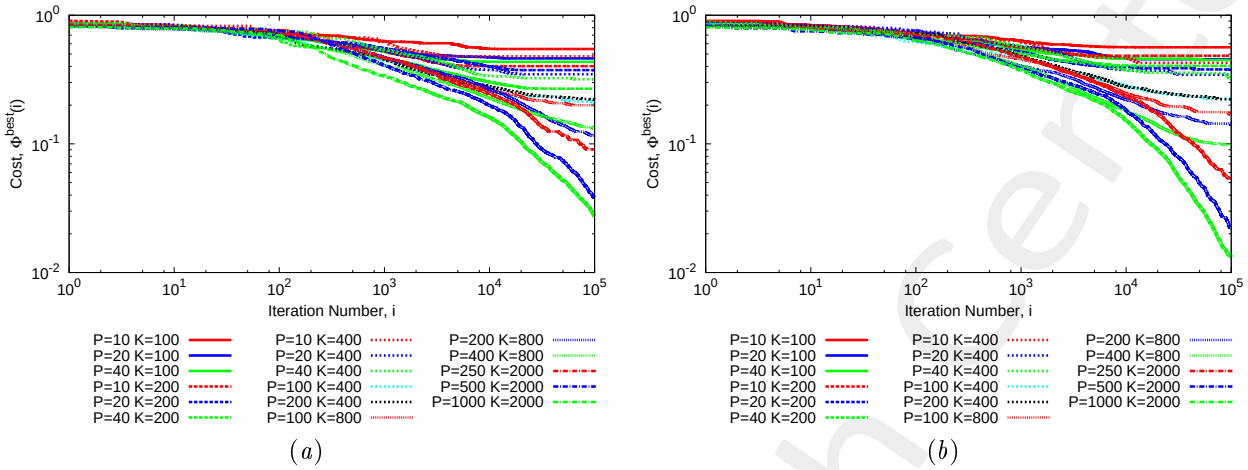

Figure 14: Cost Function behaviour at different population and number of coefficient for Seed=1(a) and Seed=2(b).

Observations:

- The cost function is lower for the test cases that involve the higher number of coefficient and the higher population;
- In Fig. 14 it is shown that the cost function is decreased increasing the number of iteration;
- the cases with the lower population (or better with a low ratio between the number of unknown K and the population dimension P) have worse results.
- the best result is obtained for $K = 2000$, $P = 1000$, Random Seed = 2.

1.6 Number of Coefficient K calibration

We set the number of particle equal to the ten percent of the number of unknowns so:

- number of unknowns: $U = 2 \times K$;
- $P = 10\%U$;
- $I = 3 \times 10^5$;

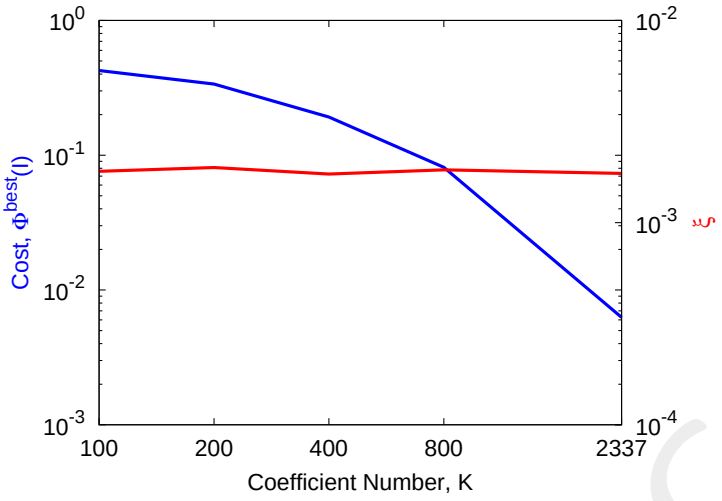

Figure 15: Final Cost Function and Integral error behaviour at different number of Coefficient selected (K).

We can notice that:

1. the final value of the cost function is lower as we select all the possible coefficient;
2. the Integral error on the radiated field is almost the same varying the number of coefficient.

1.7 K=2000, P=250, I=100000, 20 seed

In this Section is increased the number of seed in order to have a statistical behaviour of the test case with the population almost at 6% of the number of coefficients.

In the Fig. 16 is depicted the behaviour of the Cost Function varying the random seed. The best value of cost function is achieved by Seed=17 and is $\Phi = 3.585 \times 10^{-2}$.

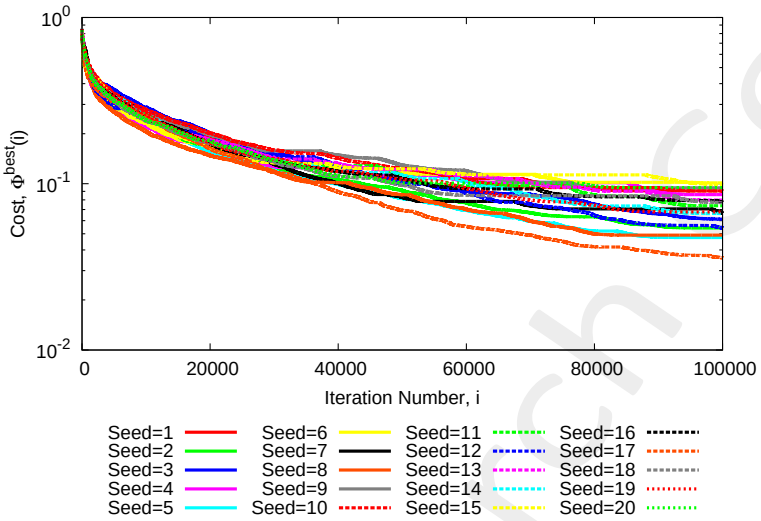

Figure 16: Cost Function behaviour at different random seed.

At this value of cost function the achieved performance on the Phase are showed in Fig. 17 and are numerically showed in table IX.

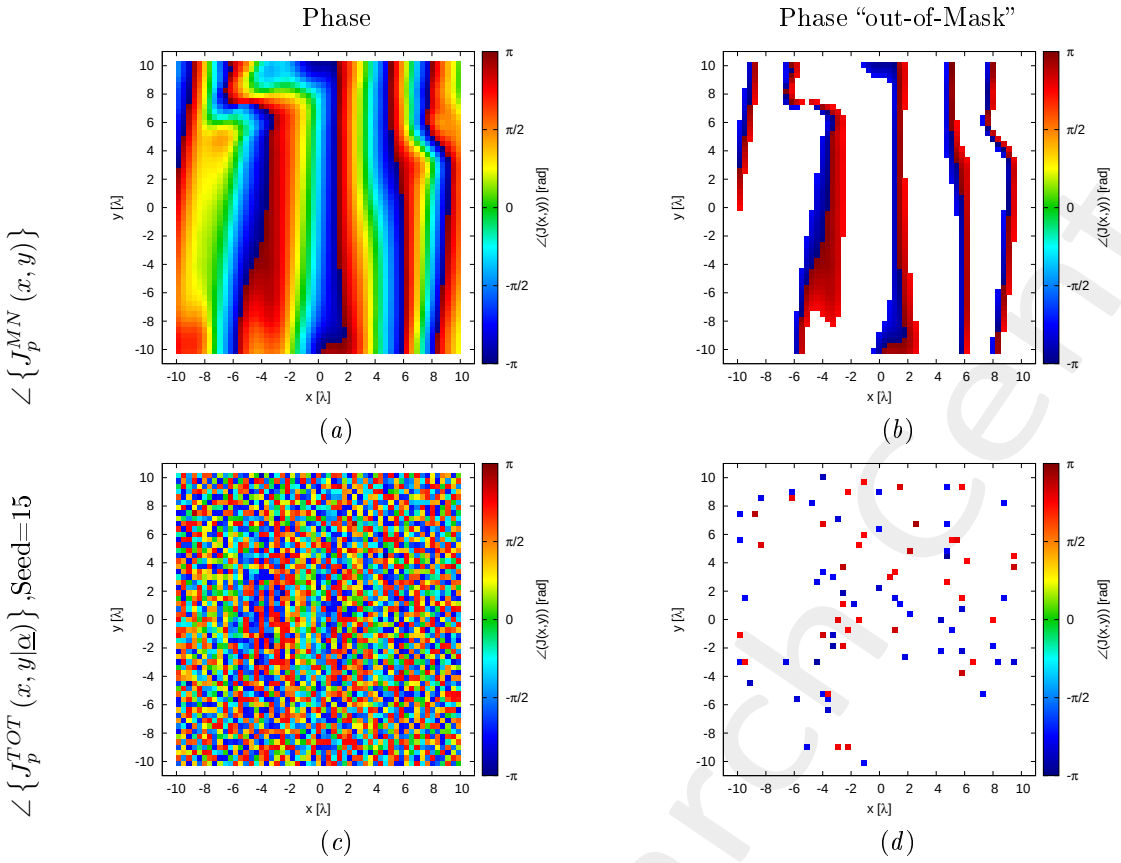

Figure 17: Phase $(a)(c)(e)$ and value of the phase out of the minimization range $(b)(d)(f)$ of the Minimum-Norm current $(\angle\{J_p^{MN}(x,y)\})(a)(b)$, of the total current for the best random seed = 17$(c)(d)$.

Case	Φ	Number of value $> \phi_p^{MAX}(x,y)$	Number of value$< \phi_p^{MIN}(x,y)$	Phase Range		Time $[s]$	
				Min $[deg]$	Max $[deg]$	parallel	no-parallel
MN	1.0	899	663	-179.87	179.63		
Seed=15	3.585×10^{-2}	37	47	-170.36	164.29	1.89×10^5	1.43×10^6

Table IX: Cost Function value and statistics about the result.

The verification of the radiated field is showed in Fig. 18 and numerically in table X.

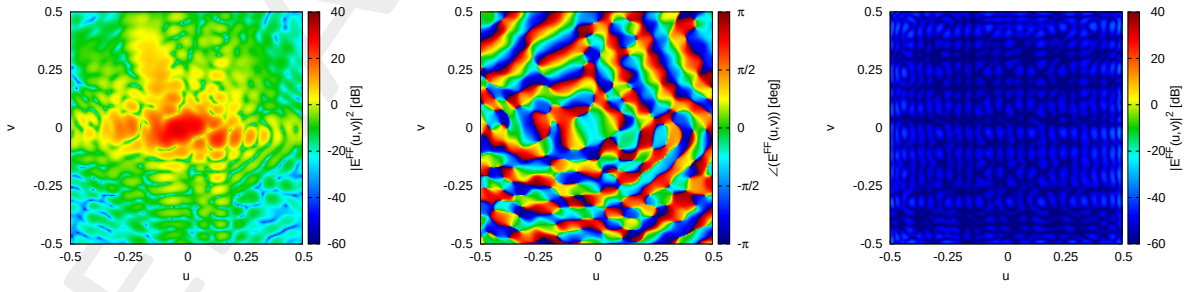

Figure 18: Magnitude (a), Phase (b) and Magnitude of the difference with respect to the original field (c) of the seed=17 $(a)(b)(c)$.

Seed	ξ
17	1.98×10^{-3}

Table X: Integral error of the difference between the original field and the one radiated by the total current.

Moreover, the statistics on the cost function with different seed is descried in Tab. XI

Average Φ	Minimum Φ	Maximum Φ	Median Φ	Variance Φ
7.221×10^{-2}	3.585×10^{-2}	1.012×10^{-1}	7.370×10^{-2}	3.340×10^{-4}

Table XI: Cost function statistics.

2 Phase Range [-150:150] - Test Case 1 - 55x55 - Linear Polarization

This section is aimed at showing the result of setting the wanted phase range to $[-150, 150]$ using a PSO with different parameters.

2.1 Parameters

- Reflectarray Geometry:
  - number of elements along x: $M = 55$;
  - number of elements along y: $N = 55$;
  - element spacing along x: $\Delta x = 0.373333$ $[\lambda]$;
  - element spacing along y: $\Delta y = 0.373333$ $[\lambda]$;
  - non radiating dimension: 2337;
  - truncation order: $H = 688$;
- PSO Parameters
  - max iteration number: $I = \{10^5, 1.5 \times 10^5, 3 \times 10^5\}$;
  - number of NR-Basis: $K = 2000$;
  - swarm size: $P = K \times 2 \times 10\% = 400$ ($\times 2$ real and imaginary part);
  - inertial weight: 0.4;
  - inertial: 2 -> consider constant inertial velocity;
  - alpha: 0.4,
  - beta: 0.4;
  - c1: 2.0;
  - c2: 2.0;
  - random seed: {1, 2}.
- Optimization Parameters
  - $\phi_q^{MAX}(x, y) = 150$ $[deg]$;
  - $\phi_q^{MIN}(x, y) = -150$ $[deg]$;
  - $\min\{\Re\{\underline{\alpha}\}\} = -1.0$;
  - $\max\{\Re\{\underline{\alpha}\}\} = 1.0$;
  - $\min\{\Im\{\underline{\alpha}\}\} = -1.0$;
  - $\max\{\Im\{\underline{\alpha}\}\} = 1.0$.

Initialialization We use a population with:

- an agent with the $\underline{\alpha} = \underline{0}$,
- all the other agents with random initialized $\underline{\alpha}$.

2.2 Results - K=2000 - Iteration 100k

In the Fig. 19 is depicted the behaviour of the Cost Function varying the random seed. The best value of cost function is achieved by Seed=1 and is $\Phi = 1.411 \times 10^{-3}$.

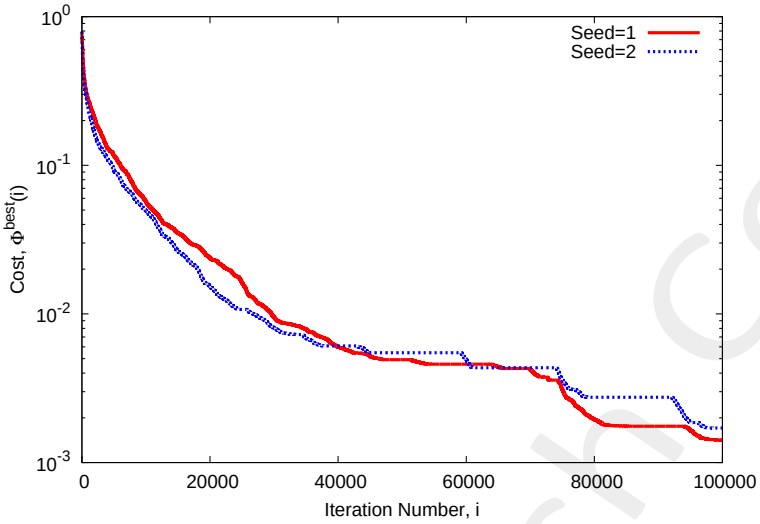

Figure 19: Cost Function behaviour at different random seed.

At this value of cost function the achieved performance on the Phase are showed in Figs. 20,21 and are numerically showed in table XII.

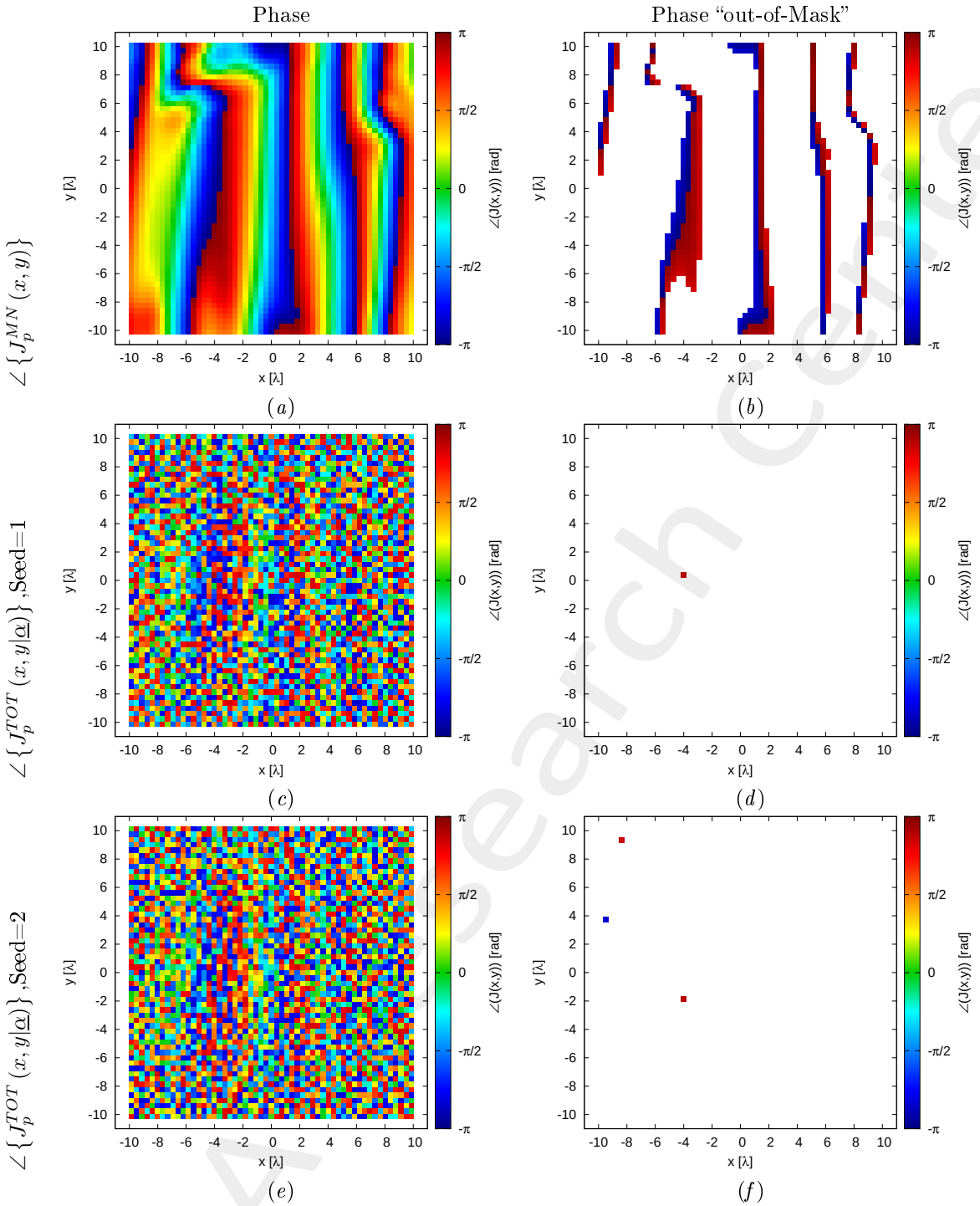

Figure 20: Phase $(a)(c)(e)$ and value of the phase out of the minimization range $(b)(d)(f)$ of the Minimum-Norm current $(\angle\{J_p^{MN}(x,y)\})(a)(b)$, of the total current for the random seed $= 1(c)(d)$ and for the random seed $= 2(e)(f)$.

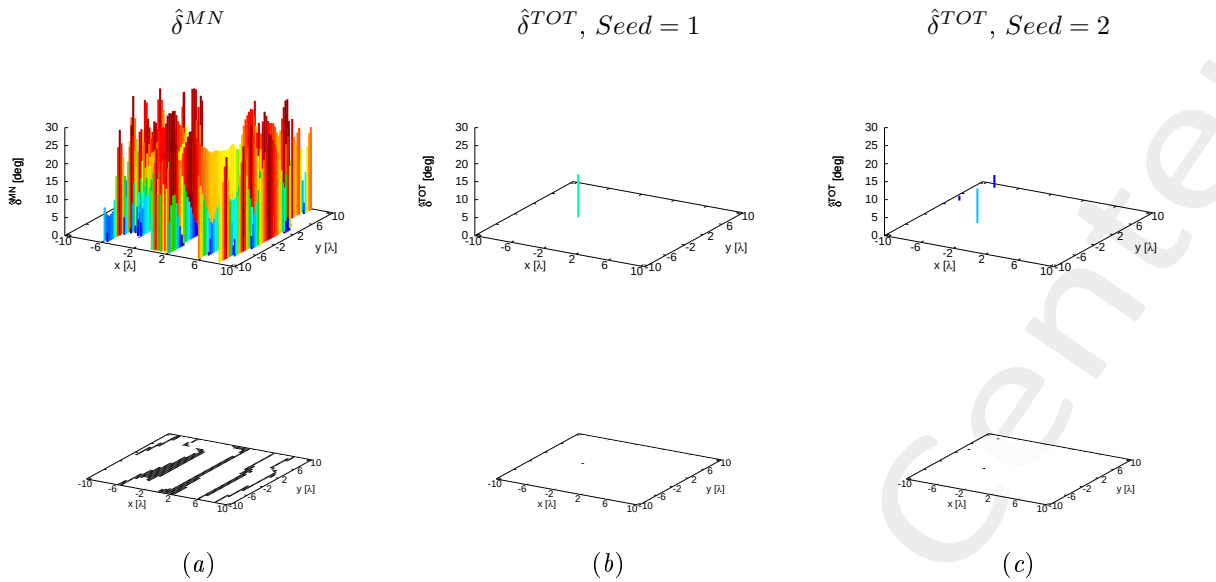

Figure 21: Phase Mask mismatch for the Minimum-Norm current (a), the total current for the random seed $= 1(b)$, and for the random seed $= 2(c)$.

Case	Φ	Number of value $> \phi_p^{MAX}(x,y)$	Number of value $< \phi_p^{MIN}(x,y)$	Phase Range		Time $[s]$
				Min $[deg]$	Max $[deg]$	
MN	1.0	310	258	-179.87	179.63	
Seed=1	1.411×10^{-3}	1	0	-150.00	161.98	4.25×10^5
Seed=2	1.709×10^{-3}	2	1	-151.34	159.63	4.24×10^5

Table XII: Cost Function value and statistics about the result.

The verification of the radiated field is showed in Fig. 22 and numerically in table XIII.

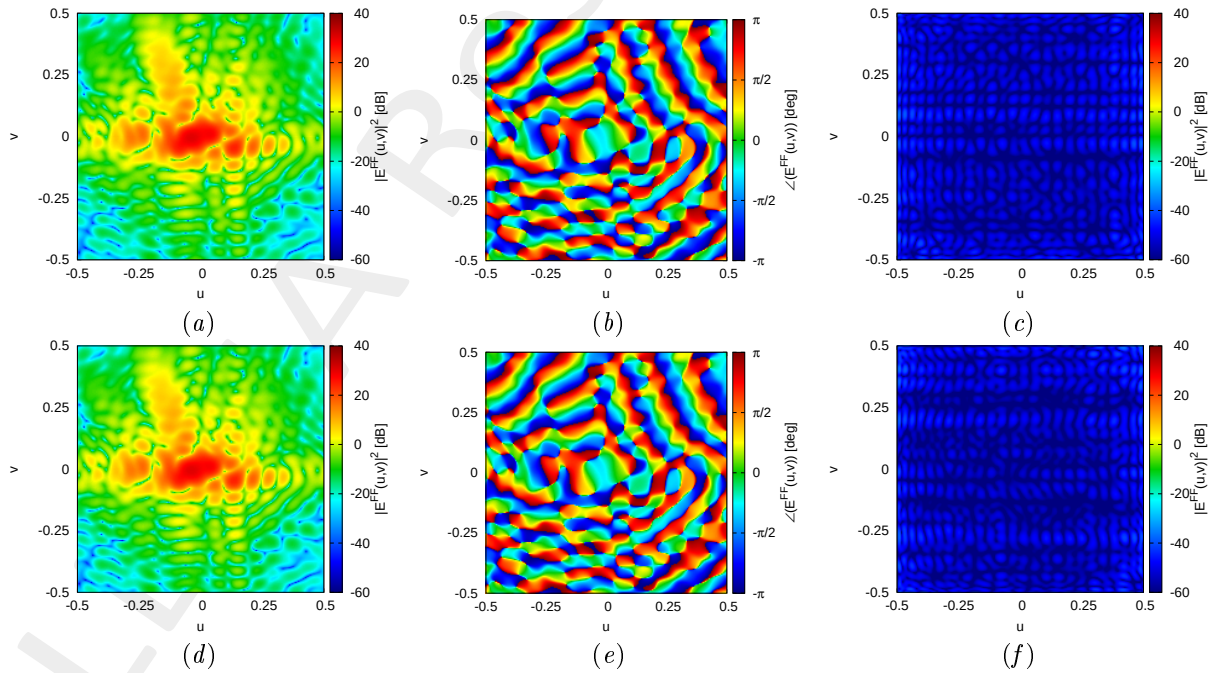

Figure 22: Magnitude $(a)(d)$, Phase $(b)(e)$ and Magnitude of the difference with respect to the original field $(c)(f)$ of the seed=1 $(a)(b)(c)$ and seed=2 $(d)(e)(f)$.

Seed	ξ
1	1.89×10^{-3}
2	1.79×10^{-3}

Table XIII: Integral error of the difference between the original field and the one radiated by the total current.

2.3 Results - K=2000 - Iteration 150k

In the Fig. 23 is depicted the behaviour of the Cost Function varying the random seed. The best value of cost function is achieved by Seed=2 and is $\Phi = 1.023 \times 10^{-3}$.

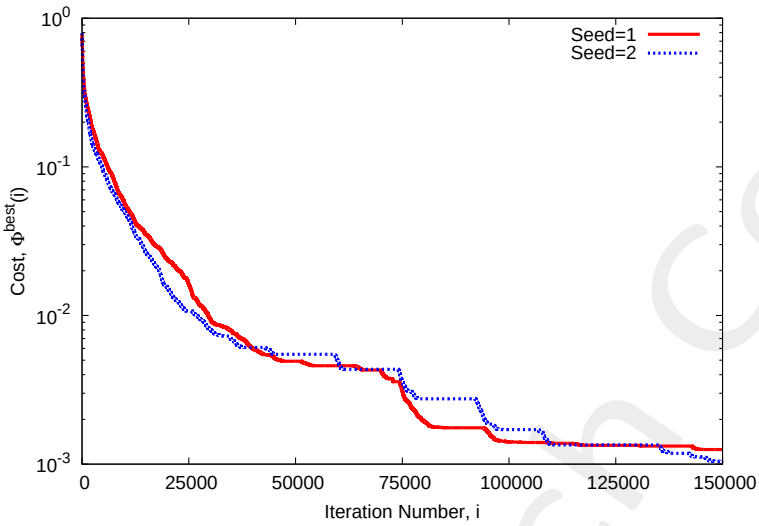

Figure 23: Cost Function behaviour at different random seed.

At this value of cost function the achieved performance on the Phase are showed in Figs. 24,25 and are numerically showed in table XIV.

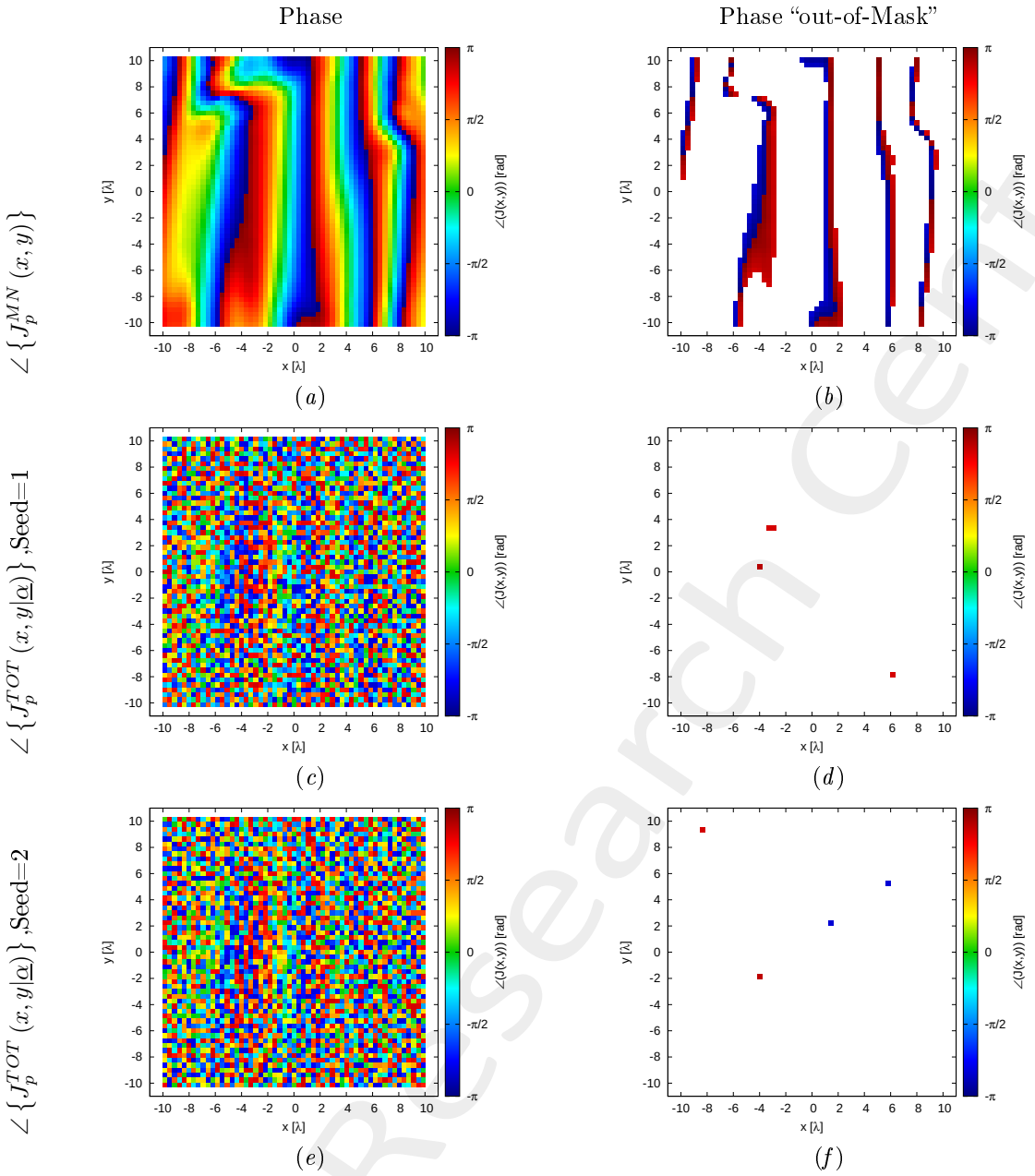

Figure 24: Phase $(a)(c)(e)$ and value of the phase out of the minimization range $(b)(d)(f)$ of the Minimum-Norm current ($\angle\{J_p^{MN}(x,y)\}$)$(a)(b)$, of the total current for the random seed $= 1(c)(d)$ and for the random seed $= 2(e)(f)$.

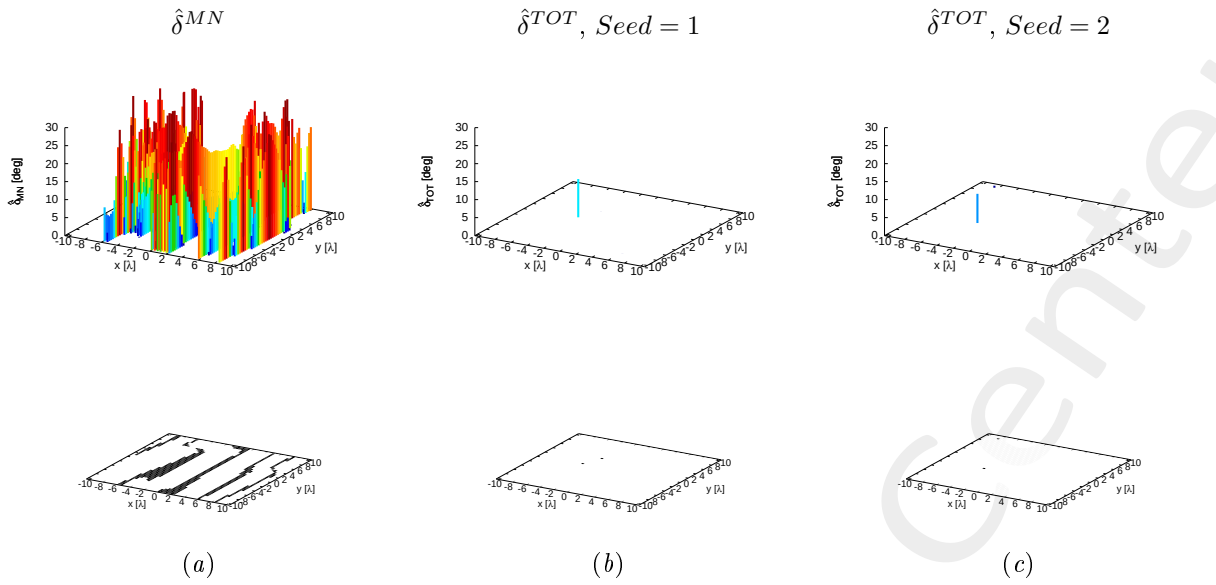

(a) (b) (c)

Figure 25: Phase Mask mismatch for the Minimum-Norm current (a), the total current for the random seed $= 1(b)$, and for the random seed $= 2(c)$.

Case	Φ	Number of value $> \phi_p^{MAX}(x,y)$	Number of value $< \phi_p^{MIN}(x,y)$	Phase Range		Time $[s]$
				Min $[deg]$	Max $[deg]$	
MN	1.0	310	258	-179.87	179.63	
Seed=1	1.255×10^{-3}	1	0	-150.00	160.62	6.75×10^5
Seed=2	1.023×10^{-3}	2	0	-150.00	158.12	8.21×10^5

Table XIV: Cost Function value and statistics about the result.

With respect at the case with 10^5 iteration the Cost Function is dereased. However, the number of element with a phase out of the mask is increased from 1 to 4, but 3/4 for seed=1 and 2/4 for seed=2 have a values of Phase Mask mismatch $(\hat{\delta})$ below 10^{-2} degrees so they are thresholded to 0.

The verification of the radiated field is showed in Fig. 26 and numerically in table XV.

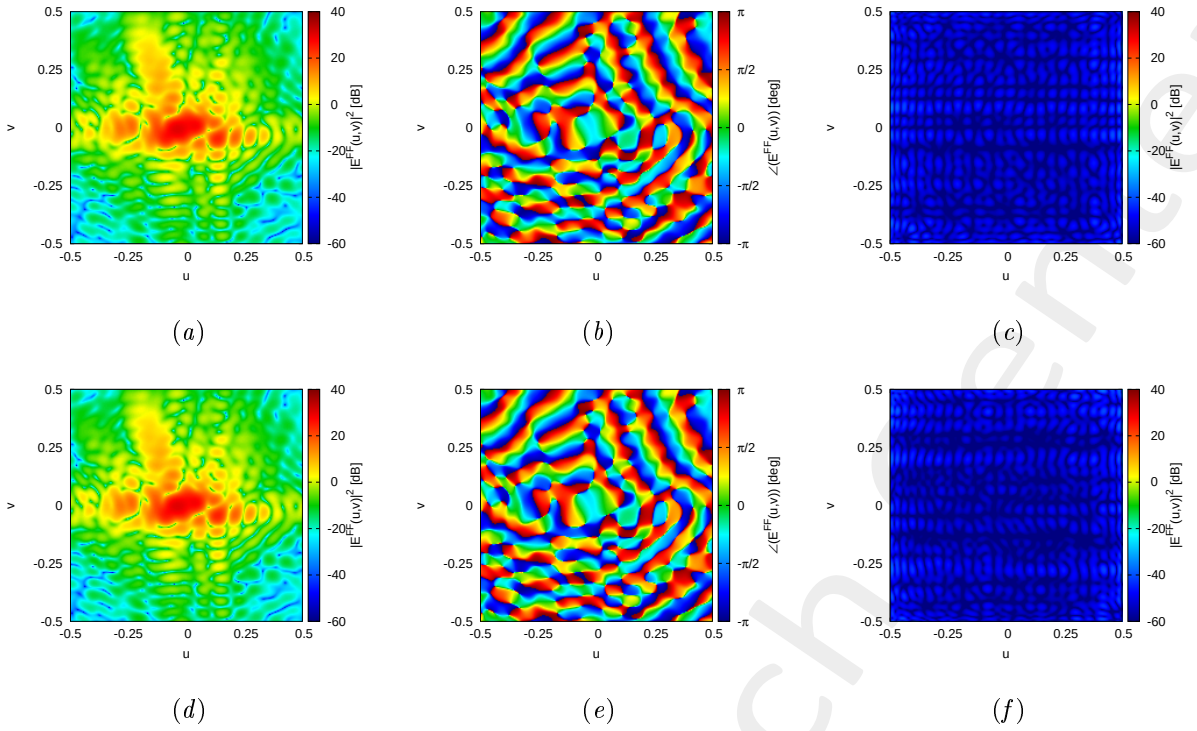

Figure 26: Magnitude $(a)(d)$, Phase $(b)(e)$ and Magnitude of the difference with respect to the original field $(c)(f)$ of the seed=1 $(a)(b)(c)$ and seed=2 $(d)(e)(f)$.

Seed	ξ
1	1.89×10^{-3}
2	1.79×10^{-3}

Table XV: Integral error of the difference between the original field and the one radiated by the total current.

2.4 Results - K=2000 - Iteration 300k

In the Fig. 27 is depicted the behaviour of the Cost Function varying the random seed. The best value of cost function is achieved by Seed=2 and is $\Phi = 1.614 \times 10^{-4}$.

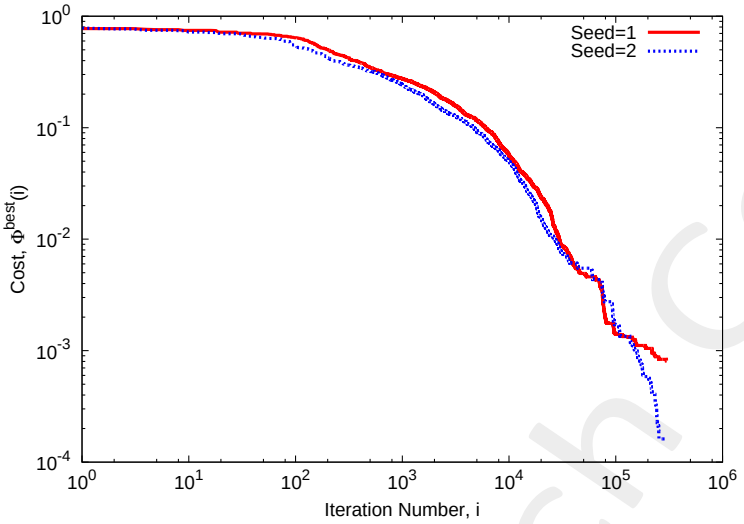

Figure 27: Cost Function behaviour at different random seed.

At this value of cost function the achieved performance on the Phase are showed in Figs. 28,29 and are numerically showed in table XVI.

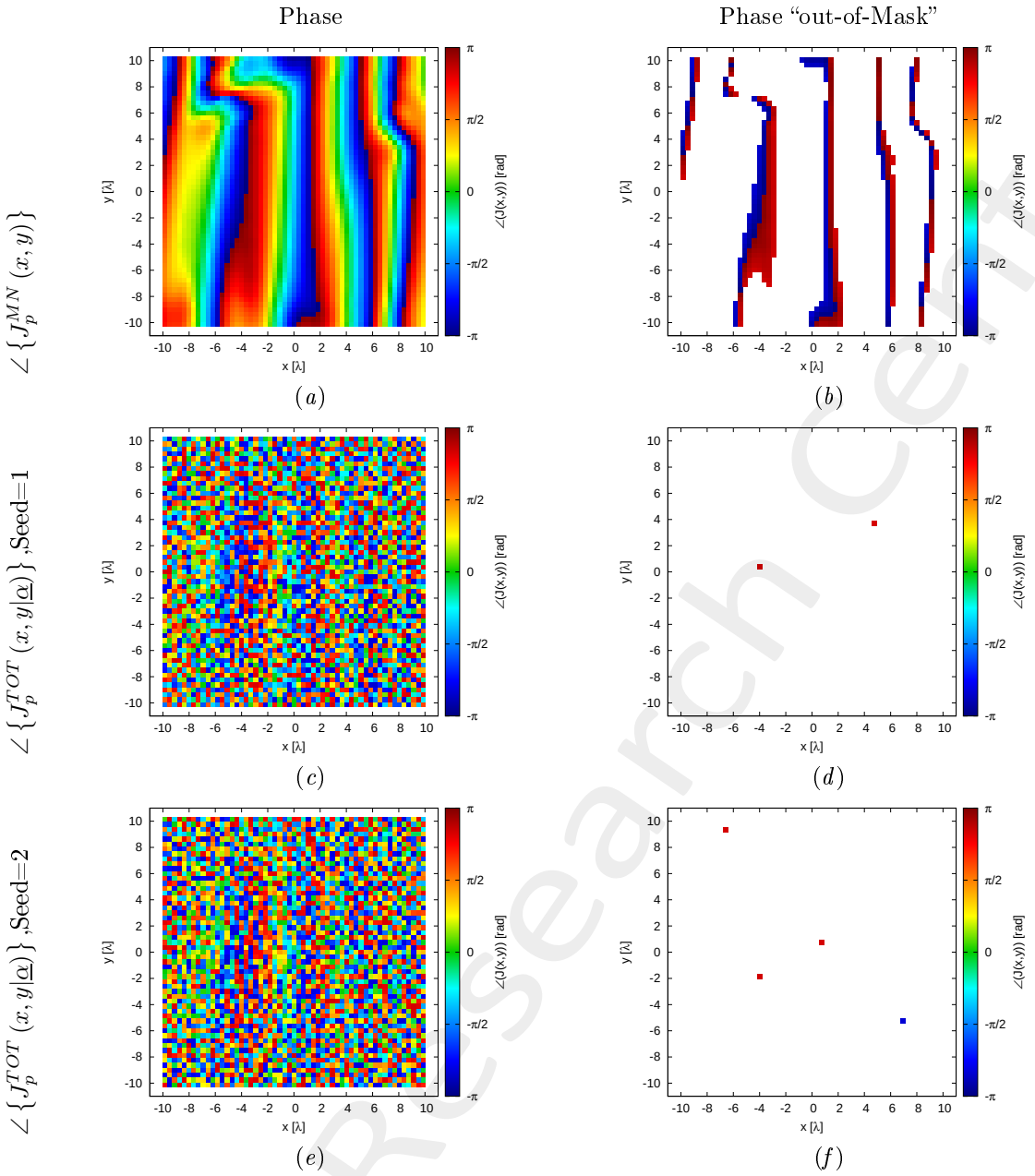

Figure 28: Phase $(a)(c)(e)$ and value of the phase out of the minimization range $(b)(d)(f)$ of the Minimum-Norm current ($\angle\{J_p^{MN}(x,y)\}$)$(a)(b)$, of the total current for the random seed $= 1(c)(d)$ and for the random seed $= 2(e)(f)$.

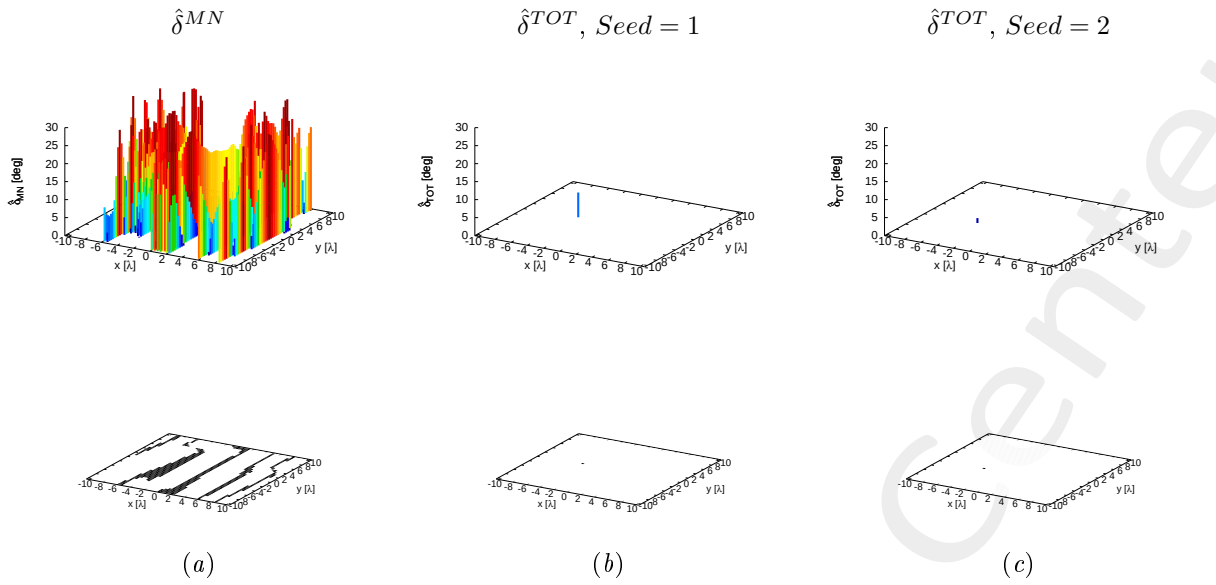

(a) (b) (c)

Figure 29: Phase Mask mismatch for the Minimum-Norm current (a), the total current for the random seed $= 1(b)$, and for the random seed $= 2(c)$.

Case	Φ	Number of value $> \phi_p^{MAX}(x,y)$	Number of value $< \phi_p^{MIN}(x,y)$	Phase Range		Time $[s]$
				Min $[deg]$	Max $[deg]$	
MN	1.0	310	258	-179.87	179.63	
Seed=1	8.094×10^{-4}	1	0	-150.00	156.82	1.42×10^6
Seed=2	1.614×10^{-4}	1	0	-150.00	151.37	1.41×10^6

Table XVI: Cost Function value and statistics about the result.

The verification of the radiated field is showed in Fig. 30 and numerically in table XVII.

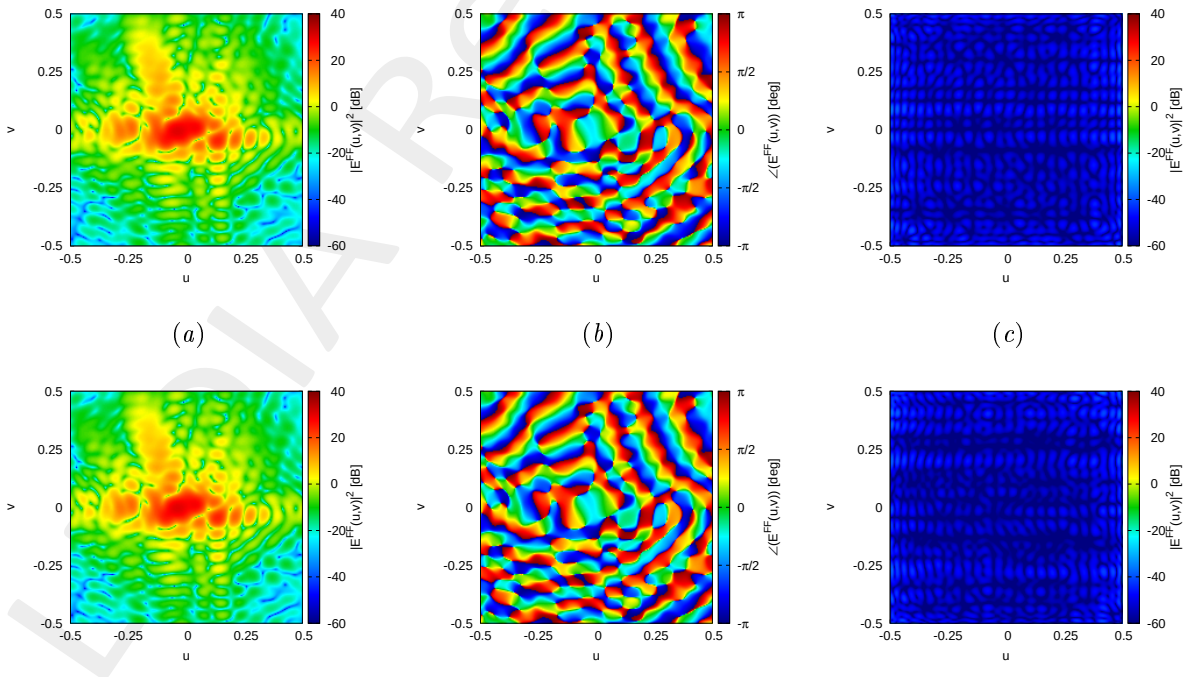

(a) (b) (c)

(d) (e) (f)

Figure 30: Magnitude $(a)(d)$, Phase $(b)(e)$ and Magnitude of the difference with respect to the original field $(c)(f)$ of the seed=1 $(a)(b)(c)$ and seed=2 $(d)(e)(f)$.

Seed	ξ
1	1.88×10^{-3}
2	1.78×10^{-3}

Table XVII: Integral error of the difference between the original field and the one radiated by the total current.

More information on the topics of this document can be found in the following list of references.

References

[1] M. Salucci, G. Oliveri, M. A. Hannan, and A. Massa, "System-by-design paradigm-based synthesis of complex systems: The case of spline-contoured 3D radomes," *IEEE Antennas and Propagation Magazine - Special Issue on 'Artificial Intelligence in Electromagnetics,'*, vol. 64, no. 1, pp. 72-83, Feb. 2022.

[2] G. Oliveri, P. Rocca, M. Salucci, and A. Massa, "Holographic smart EM skins for advanced beam power shaping in next generation wireless environments," *IEEE J. Multiscale Multiphysics Comput. Tech.*, vol. 6, pp. 171-182, Oct. 2021.

[3] G. Oliveri, A. Gelmini, A. Polo, N. Anselmi, and A. Massa, "System-by-design multi-scale synthesis of task-oriented reflectarrays," *IEEE Trans. Antennas Propag.*, vol. 68, no. 4, pp. 2867-2882, Apr. 2020.

[4] M. Salucci, L. Tenuti, G. Gottardi, A. Hannan, and A. Massa, "System-by-design method for efficient linear array miniaturisation through low-complexity isotropic lenses," *Electronic Letters*, vol. 55, no. 8, pp. 433-434, May 2019.

[5] M. Salucci, N. Anselmi, S. Goudos, and A. Massa, "Fast design of multiband fractal antennas through a system-by-design approach for NB-IoT applications," *EURASIP J. Wirel. Commun. Netw.*, vol. 2019, no. 1, pp. 68-83, Mar. 2019.

[6] M. Salucci, G. Oliveri, N. Anselmi, and A. Massa, "Material-by-design synthesis of conformal miniaturized linear phased arrays," *IEEE Access*, vol. 6, pp. 26367-26382, 2018.

[7] M. Salucci, G. Oliveri, N. Anselmi, G. Gottardi, and A. Massa, "Performance enhancement of linear active electronically-scanned arrays by means of MbD-synthesized metalenses," *Journal of Electromagnetic Waves and Applications*, vol. 32, no. 8, pp. 927-955, 2018.

[8] G. Oliveri, M. Salucci, N. Anselmi and A. Massa, "Multiscale System-by-Design synthesis of printed WAIMs for waveguide array enhancement," *IEEE J. Multiscale Multiphysics Computat. Techn.*, vol. 2, pp. 84-96, 2017.

[9] A. Massa and G. Oliveri, "Metamaterial-by-Design: Theory, methods, and applications to communications and sensing - Editorial," *EPJ Applied Metamaterials*, vol. 3, no. E1, pp. 1-3, 2016.

[10] G. Oliveri, F. Viani, N. Anselmi, and A. Massa, "Synthesis of multi-layer WAIM coatings for planar phased arrays within the system-by-design framework," *IEEE Trans. Antennas Propag.*, vol. 63, no. 6, pp. 2482-2496, June 2015.

[11] G. Oliveri, L. Tenuti, E. Bekele, M. Carlin, and A. Massa, "An SbD-QCTO approach to the synthesis of isotropic metamaterial lenses," *IEEE Antennas Wireless Propag. Lett.*, vol. 13, pp. 1783-1786, 2014.

[12] A. Massa, G. Oliveri, P. Rocca, and F. Viani, "System-by-Design: a new paradigm for handling design complexity," *8th European Conference on Antennas Propag. (EuCAP 2014), The Hague, The Netherlands*, pp. 1180-1183, Apr. 6-11, 2014.

[13] P. Rocca, M. Benedetti, M. Donelli, D. Franceschini, and A. Massa, "Evolutionary optimization as applied to inverse problems," *Inverse Problems - 25 th Year Special Issue of Inverse Problems, Invited Topical Review*, vol. 25, pp. 1-41, Dec. 2009.

[14] P. Rocca, G. Oliveri, and A. Massa, "Differential Evolution as applied to electromagnetics," *IEEE Antennas Propag. Mag.*, vol. 53, no. 1, pp. 38-49, Feb. 2011.

[15] M. Salucci, G. Gottardi, N. Anselmi, and G. Oliveri, "Planar thinned array design by hybrid analytical-stochastic optimization," *IET Microwaves, Antennas & Propagation*, vol. 11, no. 13, pp. 1841-1845, Oct. 2017

[16] G. Oliveri, M. Donelli, and A. Massa, "Genetically-designed arbitrary length almost difference sets," *Electronics Letters*, vol. 5, no. 23, pp. 1182-1183, Nov. 2009.

[17] P. Rocca, N. Anselmi, A. Polo, and A. Massa, "Pareto-optimal domino-tiling of orthogonal polygon phased arrays," *IEEE Trans. Antennas Propag.*, vol. 70, no. 5, pp. 3329-3342, May 2022.

[18] P. Rocca, N. Anselmi, A. Polo, and A. Massa, "An irregular two-sizes square tiling method for the design of isophoric phased arrays," *IEEE Trans. Antennas Propag.*, vol. 68, no. 6, pp. 4437-4449, Jun. 2020.

[19] P. Rocca, N. Anselmi, A. Polo, and A. Massa, "Modular design of hexagonal phased arrays through diamond tiles," *IEEE Trans. Antennas Propag.*, vol.68, no. 5, pp. 3598-3612, May 2020.

[20] N. Anselmi, L. Poli, P. Rocca, and A. Massa, "Design of simplified array layouts for preliminary experimental testing and validation of large AESAs," *IEEE Trans. Antennas Propag.*, vol. 66, no. 12, pp. 6906-6920, Dec. 2018.

[21] N. Anselmi, P. Rocca, M. Salucci, and A. Massa, "Contiguous phase-clustering in multibeam-on-receive scanning arrays," *IEEE Trans. Antennas Propag.*, vol. 66, no. 11, pp. 5879-5891, Nov. 2018.

[22] G. Oliveri, G. Gottardi, F. Robol, A. Polo, L. Poli, M. Salucci, M. Chuan, C. Massagrande, P. Vinetti, M. Mattivi, R. Lombardi, and A. Massa, "Co-design of unconventional array architectures and antenna elements for 5G base station," *IEEE Trans. Antennas Propag.*, vol. 65, no. 12, pp. 6752-6767, Dec. 2017.

[23] N. Anselmi, P. Rocca, M. Salucci, and A. Massa, "Irregular phased array tiling by means of analytic schemata-driven optimization," *IEEE Trans. Antennas Propag.*, vol. 65, no. 9, pp. 4495-4510, September 2017.

[24] N. Anselmi, P. Rocca, M. Salucci, and A. Massa, "Optimization of excitation tolerances for robust beamforming in linear arrays," *IET Microwaves, Antennas & Propagation*, vol. 10, no. 2, pp. 208-214, 2016.

[25] P. Rocca, R. J. Mailloux, and G. Toso, "GA-Based optimization of irregular sub-array layouts for wideband phased arrays desig," *IEEE Antennas and Wireless Propag. Lett.*, vol. 14, pp. 131-134, 2015.

[26] P. Rocca, M. Donelli, G. Oliveri, F. Viani, and A. Massa, "Reconfigurable sum-difference pattern by means of parasitic elements for forward-looking monopulse radar," *IET Radar, Sonar & Navigation*, vol 7, no. 7, pp. 747-754, 2013.

[27] P. Rocca, L. Manica, and A. Massa, "Ant colony based hybrid approach for optimal compromise sum-difference patterns synthesis," *Microwave Opt. Technol. Lett.*, vol. 52, no. 1, pp. 128-132, Jan. 2010.

[28] P. Rocca, L. Manica, and A. Massa, "An improved excitation matching method based on an ant colony optimization for suboptimal-free clustering in sum-difference compromise synthesis," *IEEE Trans. Antennas Propag.*, vol. 57, no. 8, pp. 2297-2306, Aug. 2009.

[29] P. Rocca, L. Manica, and A. Massa, "Hybrid approach for sub-arrayed monopulse antenna synthesis," *Electronics Letters*, vol. 44, no. 2, pp. 75-76, Jan. 2008.

[30] P. Rocca, L. Manica, F. Stringari, and A. Massa, "Ant colony optimization for tree-searching based synthesis of monopulse array antenna," *Electronics Letters*, vol. 44, no. 13, pp. 783-785, Jun. 19, 2008.

[31] M. Salucci, F. Robol, N. Anselmi, M. A. Hannan, P. Rocca, G. Oliveri, M. Donelli, and A. Massa, "S-Band spline-shaped aperture-stacked patch antenna for air traffic control applications," *IEEE Tran. Antennas Propag.*, vol. 66, no. 8, pp. 4292-4297, Aug. 2018.

[32] T. Moriyama, F. Viani, M. Salucci, F. Robol, and E. Giarola, "Planar multiband antenna for 3G/4G advanced wireless services," *IEICE Electronics Express*, vol. 11, no. 17, pp. 1-10, Sep. 2014.

[33] F. Viani, "Dual-band sierpinski pre-fractal antenna for 2.4GHz-WLAN and 800MHz-LTE wireless devices," *Progress In Electromagnetics Research C*, vol. 35, pp. 63-71, 2013.

[34] F. Viani, M. Salucci, F. Robol, and A. Massa, "Multiband fractal Zigbee/WLAN antenna for ubiquitous wireless environments," *Journal of Electromagnetic Waves and Applications*, vol. 26, no. 11-12, pp. 1554-1562. 2012.

[35] F. Viani, M. Salucci, F. Robol, G. Oliveri, and A. Massa, "Design of a UHF RFID/GPS fractal antenna for logistics management," *Journal of Electromagnetic Waves and Applications*, vol. 26, pp. 480-492, 2012.

[36] M. Salucci, L. Poli, A. F. Morabito, and P. Rocca, "Adaptive nulling through subarray switching in planar antenna arrays," *Journal of Electromagnetic Waves and Applications*, vol. 30, no. 3, pp. 404-414, February 2016

[37] T. Moriyama, L. Poli, and P. Rocca, "Adaptive nulling in thinned planar arrays through genetic algorithms," *IEICE Electronics Express*, vol. 11, no. 21, pp. 1-9, Sep. 2014.

[38] L. Poli, P. Rocca, M. Salucci, and A. Massa, "Reconfigurable thinning for the adaptive control of linear arrays," *IEEE Trans. Antennas Propag.*, vol. 61, no. 10, pp. 5068-5077, Oct. 2013.

[39] P. Rocca, L. Poli, G. Oliveri, and A. Massa, "Adaptive nulling in time-varying scenarios through time-modulated linear arrays," *IEEE Antennas Wireless Propag. Lett.*, vol. 11, pp. 101-104, 2012.

[40] F. Viani, F. Robol, M. Salucci, and R. Azaro, "Automatic EMI filter design through particle swarm optimization," *IEEE Trans. Electromagnet. Compat.*, vol. 59, no. 4, pp. 1079-1094, Aug. 2017.

[41] G. Oliveri, M. Salucci, and A. Massa, "Towards reflectarray digital twins - An EM-driven machine learning perspective," *IEEE Transactions on Antennas and Propagation - Special Issue on 'Machine Learning in Antenna Design, Modeling, and Measurements,'* vol. 70, no. 7, pp. 5078-5093, July 2022.

[42] M. Salucci, L. Tenuti, G. Oliveri, and A. Massa, "Efficient prediction of the EM response of reflectarray antenna elements by an advanced statistical learning method," *IEEE Trans. Antennas Propag.*, vol. 66, no. 8, pp. 3995-4007, Aug. 2018.